Science Bulletin 64 (2019) 1272–1279

Contents lists available at ScienceDirect

Science Bulletin

journal homepage: www.elsevier.com/locate/scib

Article

Highly sensitive and selective electrochemical immunosensors by substrate-enhanced electroless deposition of metal nanoparticles onto three-dimensional graphene@Ni foams

Changrong Zhao [a], Xiaoli Li [a], Shixia An [a], Dongliang Zheng [a], Shuaili Pei [a], Xiao Zheng [a], Yu Liu [a], Qingqing Yao [a], Mei Yang [a], Liming Dai [a,b,*]

[a] Institute of Advanced Materials for Nano-Bio Applications, School of Ophthalmology & Optometry, Wenzhou Medical University, Wenzhou 325027, China
[b] Department of Macromolecule Science and Engineering, Case Western Reserve University, Cleveland, OH 44106, USA

ARTICLE INFO

Article history:
Received 21 June 2019
Received in revised form 27 June 2019
Accepted 8 July 2019
Available online 17 July 2019

Keywords:
Electrochemical immunosensor
Substrate-enhanced electroless deposition
Graphene
Ni foam
Metal nanoparticles
α-Fetoprotein antigen

ABSTRACT

In this study, we have for the first time preformed the facile substrate-enhanced electroless deposition (SEED) of metal nanoparticles onto monolithic graphene@Ni foams for construction of disposable three-dimensional (3D) electrochemical immunosensors. Specifically, we firstly used the SEED method to deposit gold nanoparticles (AuNPs) onto the graphene@Ni foam for immobilization of antibody (Ab_1). This is followed by a second step SEED deposition to produce silver nanoparticles (AgNPs) for electrochemical stripping detection. Using α-fetoprotein antigen (AFP) as a module analyte, the newly-developed sensor showed a wide linear response, ranging from 5.0 pg/mL to 5.0 ng/mL and a low detection limit down to 2.3 pg/mL. The newly-developed 3D-immunosensor is sensitive, reliable, and easy to be fabricated, showing great potential for clinic applications.

1. Introduction

Since the level of tumor markers in serum/tissue is closely associated with the stage of the tumor, it is very important to determine the tumor markers for cancer screening and diagnosis [1,2]. In this regard, numerous immunosensors, including electrochemical sensors [3,4], electrochemiluminescence sensors [5], fluorescence sensors [6], gravimetric sensors [7], and mass spectrometric sensors [8], have been developed for the detection of various tumor markers. Among them, the electrochemical sensors have attracted considerable attention because of their unique multiple advantages (e.g., low cost, good portability, high sensitivity) [9].

The most prevalent type of electrochemical immunosensor is in a sandwich format. Typically, a sandwich electrochemical sensor is fabricated by the following procedures: (1) immobilization of capture immunoreagent onto the electrode to construct recognition interface; (2) capture target tumor markers onto the electrode by immunoreaction; and (3) bonding electrochemical signal label onto the electrode for target determination. The first step to construct the recognition interface is crucial for the development of an electrochemical immunosensor [10]. To improve the detection performance, various nanomaterials have been applied for constructing the recognition interface. This is because nanomaterials can modify the electrode to increase the conductivity and surface area for increasing the immobilization efficiency and detection sensitivity [11,12]. However, it is often a multistep process to use nanomaterials for constructing the recognition interface in a sensor [11], involving the tedious materials fabrication in solution, and subsequent deposition of thus-produced nanomaterials onto the electrode surface. During these complex processes, nanomaterials are liable to self-agglomeration or exfoliation from the electrode surface. Therefore, it is highly desirable to simplify the procedure for constructing stable nanomaterials at the recognition interface of an electrochemical immunosensor.

On the other hand, three-dimensional (3D) graphene foams prepared by chemical vapor deposition (CVD) have attracted enormous interest for electrochemical sensing [13–15]. 3D electrode materials have many advantages, including a large specific surface area, 3D multiplexed and highly conductive pathways for electron transport, well-defined microporous structures for ion diffusion, good biocompatibility and mechanical stability [13]. The large specific surface area can improve the efficiency for immobilization

* Corresponding author.
E-mail address: liming.dai@case.edu (L. Dai).

https://doi.org/10.1016/j.scib.2019.07.015
2095-9273/

antibody while the microporous structure with unhindered substance diffusion is beneficial for keeping activities of antibody and antigen. In spite of the aforementioned advantages, 3D foam electrode materials have rarely been used in immunosensors, probably because of technical difficulties associated with the 3D structure fabrication and biofunctionalization.

For the use of a 3D nickel foam as the template, the removal of the nickel substrate could influence mechanic properties of the resultant 3D electrochemical immunosensor. Besides, the foam is often difficult to be biofunctionalized due to its ultrahigh hydrophobicity [16]. Nevertheless, some satisfying results have been achieved by developing immunosensors on the 3D foams for carcinoembryonic antigen (CEA) determination. In the CEA 3D-immunosensor, polydopamine (pDA)-concanavalin A (Con A) was used as biofunction regent to immobilize sugar protein conjugated antibody (HRP-Ab) onto the foam [17]. Unfortunately, this pDA-Con A platform was only suitable for immobilizing those antibodies with sugar chains and the immobilization procedures were rather complicated.

We have previously reported that when carbon nanotubes were supported with a metal substrate of a low redox potential, metal ions with a redox potential higher than that of the supporting metal substrate could be readily reduced into metal nanoparticles onto the carbon nanotubes [18]. Accordingly, this deposition process free from any chemical reducing reagent or electrochemical circuit was designated as Substrate-Enhanced Electroless Deposition (SEED) [18]. Herein, we used monolithic graphene@Ni foam (3D-G@Ni) as the free-standing disposable low-redox-potential (Ni^{2+}/Ni, −0.257 V vs. standard hydrogen electrode, SHE) substrate for constructing a three-dimensional (3D) electrochemical immunosensor by using this facile SEED method. When high-redox-potential metal ions, $AuCl_4^-$ ($AuCl_4^-$/Au, +1.002 V vs. SHE) or Ag^+ (Ag+/Ag, +0.799 V vs. SHE) dropping onto the graphene@Ni foam, graphene acted as a cathode for AuNPs or AgNPs deposition by reducing $AuCl_4^-$ or Ag^+ in solution, while the metal substrate Ni served as an anode where metal atoms Ni were oxidized into Ni^{2+} [18]. As schematically shown in Scheme 1, the 3D-immunosensor interface was fabricated via only two steps. Firstly, Au nanoparticles (AuNPs) were deposited in situ onto the electrode by the SEED method. Then, α-fetoprotein capture antibodies (Ab_1) were immobilized on the electrode surface through AuNPs. For immunoassay, α-fetoprotein antigen (AFP) and AFP antibody functionalized silica nanoprobe (SiO_2/Ab_2) were anchored on the interface through a sandwich immunoreaction to significantly enhance the sensitivity for electrochemical detection of AFP. Thereafter, an aqueous solution of $AgNO_3$ (C = 1.0 mmol/L) was dropped onto the electrode surface without involving any reducing reagent to produce Ag nanoparticles (AgNPs) through another round of the SEED process. Finally, electrochemical stripping analyses were performed to determine the amount of AgNPs formed, which is inversely proportional to the AFP concentration on the electrode (vide infra). The newly-developed sensor showed a wide linear range from 5.0 pg/mL to 5.0 ng/mL and a low detection limit down to 2.3 pg/mL for the AFP detection.

As seen in Scheme 1, the formation of AgNPs can be induced by the foam via the SEED process, and the formation progress can be greatly accelerated by pre-deposited AuNPs [19]. When AFP and SiO_2/Ab_2 were anchored onto the foam by sandwich immunoreaction, the bare area of the foam and the free active site of AuNPs both decreased, leading to a decreased number of the deposited AgNPs. The more number of target AFP captured onto the electrochemical immunosensor, the less number of AgNPs is. Therefore, the amount of deposited AgNPs to be measured from the AgNPs anodic stripping peak potential in KCl solution can be used as a measure for the AFP detection sensitivity since Ni was found to show no electrochemical signal under conditions for the LSV measurements (Scheme 1). Hence, the Ni substrate can be kept in all the steps shown in Scheme 1 to facilitate the SEED process and to keep good mechanical properties for efficient fabrication of the disposable electrochemical immunosensors to be developed in this study.

2. Materials and methods

2.1. Materials and reagents

Mouse monoclonal anti-AFP (Ab_1, clone No. bsm-1621) and mouse monoclonal anti-AFP (Ab_2, clone No. bsm-1622) were purchased from Beijing Biosynthesis Biotechnology Co. Ltd. (Beijing, China). AFP standard solutions in the form of commercial AFP kits were supplied by Fujirebio Diagnostics AB (Göteborg, Sweden).

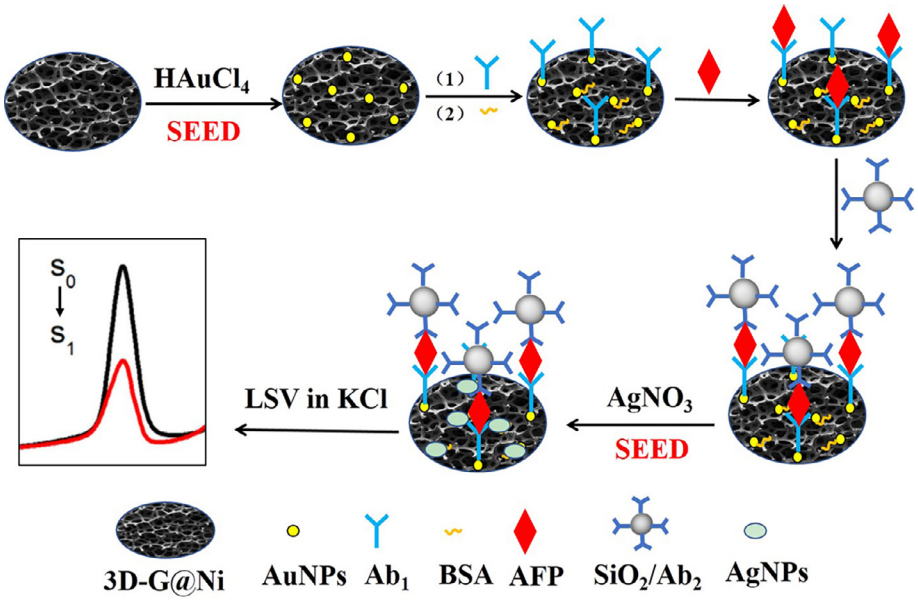

Scheme 1. (Color online) Schematic representation of the preparation procedure for constructing the immunosensor and the associated electrochemical detection strategy.

Chloroauric acid ($HAuCl_4{\cdot}4H_2O$), tetraethyl orthosilicate (TEOS), (3-aminopropyl) triethoxysilane (APTES), 1-Ethyl-3-(3′-dimethylaminopropyl) carbodiimide·HCl (EDC-HCl), and N-hydroxysuccinimide (NHS) were purchased from Sigma-Aldrich Chemical Co. (St. Louis, MO). Nickel foams were purchased from Advanced Technology Materials Co., Ltd. (Dalian, China).

Phosphate buffered saline (PBS, 0.01 mol/L, pH 7.4) was prepared and used as the buffer solution. PBS containing 5% (w/v) bovine serum albumin (BSA) was used as the blocking solution. PBS and ultrapure water were used as washing solutions in different immunoassay steps. Ultrapure water obtained from a Millipore water purification system (≥18 MΩ, Milli-Q, Millipore) was used in the whole assay. Clinical serum samples were supplied by the Second Affiliated Hospital of Wenzhou Medical University. All other reagents were of analytical grade and used as received.

2.2. Apparatus

Scanning electron micrographs (SEM) were obtained with a Phenom Pro scanning electron microscope (Phenom World, Netherlands) at an acceleration voltage of 10 kV. IR spectra were recorded using a Nicolet 6700 Fourier-transform infrared (FTIR) spectrometer (Thermal scientific, USA). Raman spectra (excited at 532 nm) were obtained by a confocal Raman microscope (Renishaw inVia, England). X-ray photoelectron spectra (XPS) were measured with an ESCALB MKII spectrometer. All electrochemical measurements were performed on a CHI 660D electrochemical workstation (Chenhua, China).

2.3. Preparation of 3D-G@Ni electrode

The monolithic 3D-G@Ni foam was synthesized by growing graphene on Ni foam according to the reported CVD method with minor modification [16], as detailed below. Firstly, three nickel foams ((250–450) g/m^2, ($70 \times 20 \times 1$) mm^3) were heated up to 1,000 °C within 45 min under N_2 (300 standard cubic per minute, SCCM) in a quartz tube furnace and kept in situ for 5 min to clean up their surfaces. Then, H_2 (100 SCCM) was injected into the tube furnance as a reducing reagent to remove the oxides from the surface of the foams, and kept for another 5 min under N_2 flow. Subsequently, the third gas CH_4 (40 SCCM) as carbon source was injected into the furnace for growing graphene on the Ni foam under N_2 and H_2 flows. The growing process proceeded for 15 min. Finally, the monolithic 3D-G@Ni materials were obtained after cooling down to the room temperature under N_2 gas flow.

The obtained 3D-G@Ni foam was tailored into a uniform shape with the conductive region in a circle of a 3-mm in diameter and insulating region in a rectangle form ((4×2) mm^2). A copper wire was pierced and clamped with the 3D-G@Ni (cf. Fig. 1c), then sealed with Teflon and AB epoxy resin (NO.7148, deli).

2.4. Preparation of SiO_2/Ab_2 nanotag

The monodispersed SiO_2 nanospheres were firstly prepared according to a reported method [20], and then amino-functionalized by following the published procedure [21]. Thereafter, 2 mg amino-functionalized nanospheres were dispersed in 1000 μL PBS prior to reacting with Ab_2. The Ab_2 was tagged with

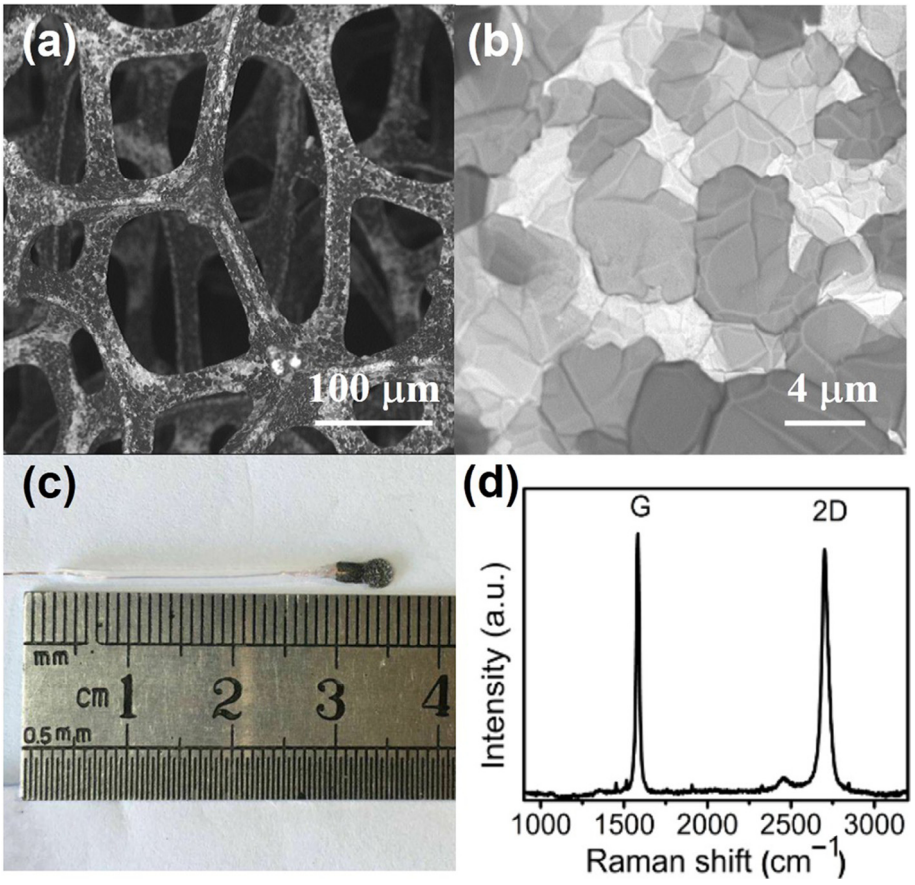

Fig. 1. (a, b) SEM images of 3D-G@Ni at different magnifications, (c) the photograph of the 3D-G@Ni electrode, and (d) Raman spectrum of the graphene grown on the Ni foam.

amino-functionalized nanospheres at room temperature by amidation reaction. Firstly, 10 μg Ab_2 was diluted by 300 μL water and activated by adding 10 μL of freshly prepared aqueous EDC-NHS, in which EDC and NHS were 3 and 6 mmol/L, respectively. After 20 min stirring, the solution of amino-functionalized nanospheres was added into the activated Ab_2 solution and stirred for 2 h. Then, the resultant mixture solution was centrifuged to obtain the precipitate, which was washed with PBS, redispersed in 1,000 μL of PBS, and blocked with 125 μL PBS solution containing 10% BSA for 30 min. After further centrifugation and washing with PBS for 3 times, the final SiO_2/Ab_2 nanotags were obtained and redispersed in 1,000 μL PBS containing 0.2% BSA at 4 °C prior to subsequent testing.

2.5. Preparation of AFP sensor

The 3D AFP senor was prepared by the SEED method at room temperature. Briefly, 1 μL ethanol was dropped onto the 3D-G@Ni electrode and then 8 μL of 0.1 mmol/L $HAuCl_4$ aqueous was immediately dropped onto the electrode for 20 min for the SEED deposition of AuNPs. Then, the electrode was washed with ultrapure water. Subsequently, 8 μL of 10 μg/mL Ab_1 solution was dropped onto the electrode surface and incubated in 100% moisture saturated environment overnight. After drying in the room moisture environment, 10 μL of 5% BSA solution was dropped onto the electrode and incubated in 100% moisture saturated environment for 1 h to block nonspecific bonding sites. Finally, the electrode was washed with PBS and the immunosensor was obtained.

2.6. Immunoassay procedure

The immunoassay procedure was carried out based on sandwich immunoreaction at 37 °C. Firstly, the immunosensor was incubated with 8 μL of AFP standard solution or serum samples for 30 min, followed by washing with PBS. Then, an 8 μL SiO_2/Ab_2 nanotag solution was casted onto the immunosensor surface for another 40 min incubation. After washing with ultrapure water, 10 μL of 1 mmol/L $AgNO_3$ solution was dropped on the immunosensor and deposited for 5 min in dark incubator at 37 °C. After another washing step with ultrapure water, the immunosensor was carried out with linear sweep voltammetry (LSV) from 0.05 to 0.15 V at 50 mV/s in 1.0 mol/L KCl solution.

3. Results and discussion

3.1. Characterization of the 3D-G@Ni

The characterization of the 3D-G@Ni was firstly performed by SEM. As shown in Fig. 1a, the 3D-G@Ni foam exhibits well-defined macroporous structure with the pore diameter of 100–300 μm. Under a higher magnification (Fig. 1b), the surface of the foam exhibits obvious wrinkles and ripples, though a relatively smooth surface was seen for each of the individual graphene pieces, as is the case for typical CVD-grown graphene [22]. Fig. 1c shows a photograph of the 3D-G@Ni electrode while Fig. 1d reproduces the corresponding Raman spectra, showing two prominent characteristic peaks at ~1,580 and ~2,700 cm^{-1} attributable to the G and 2D band of graphene, respectively [23]. The intensity ratio of the G and 2D band indicates that the graphene grown on the Ni foam was few layers [24,25].

3.2. Characterization of the nanotag

The morphologies of the SiO_2 and amino-functionalized SiO_2 were characterized by SEM and the successful attachment of Ab_2 on the amino-functionalized SiO_2 was confirmed by FTIR measurements (Fig. S1 online). The detailed results and discussion about the characterization of the nanotag were shown in the Supplementary data.

3.3. Characterization of the immunoassay

The changes of the chemical elements on the immunosensor surface in different steps were investigated by XPS. The survey spectra for the immunosensor at different fabrication stages were shown in Fig. 2a, while the high-resolution XPS spectrum of Au 4f corresponding to curve i of Fig. 2a and Ag 3d corresponding to curve iv of Fig. 2a were shown in Fig. 2b and c, respectively. Fig. 2a (curve i) and Fig. 2b show four obvious peaks (353, 335, 87.6, 83.7 eV) attributable to Au^0 ($4d_{3/2}$, $4d_{5/2}$, $4f_{5/2}$, $4f_{7/2}$) [26,27], indicating the successful deposition of the AuNPs on the foam. Compared with curve i, the appearance of a new N1s peak at 399 eV in curve ii [28] indicates the successful immobilization of the protein Ab_1 onto the foam. Meanwhile, the peak intensity of Au decreased sharply in curve ii. This is because Ab_1 was bonded with AuNPs and the XPS detection depth allows for probing only the outermost region of the Ab_1-coated AuNPs. Since the proteins

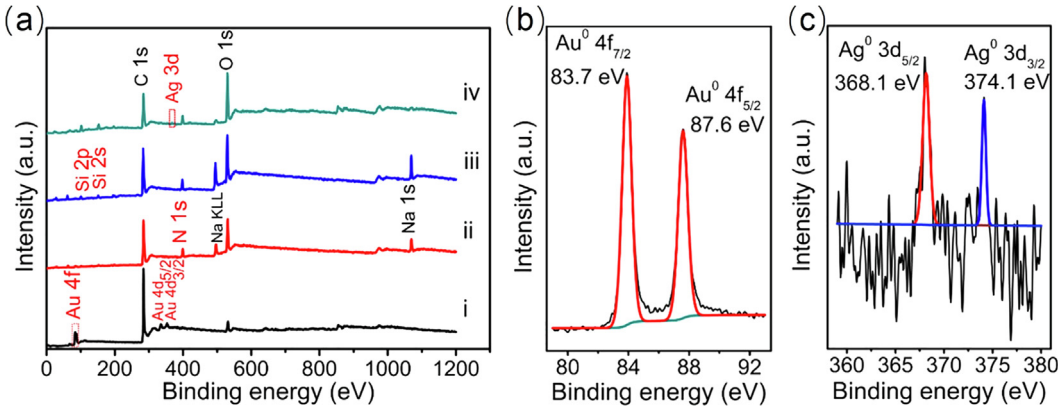

Fig. 2. (Color online) (a) XPS survey spectra of the (i) Au-deposited 3D-G@ Ni foam, (ii) after the Ab_1 immobilization, (iii) after the formation of sandwich immunocomplex, (iv) followed by silver-deposition; (b) high-resolution XPS spectrum of Au 4f in (a) (curve i); (c) high-resolution XPS spectrum of Ag 3d in (a) (curve iv). The concentrations of Ab_1, AFP, and SiO_2/Ab_2 were 10 μg/mL, 5 ng/mL and 10 μg/mL (according to the Ab_2 amount used for preparing nanotag), respectively; the incubation time for AFP and SiO_2/Ab_2 were 30 and 40 min, respectively.

(Ab_1, AFP and Ab_2) were anchored on the foam in subsequent immunoassay steps, curves iii and iv in Fig. 2a show further increases in the N 1s peak intensity and further decreases in the Au peak intensity. Meanwhile, the Si 2s (154 eV) and Si 2p (103 eV) peaks appeared in curves iii and iv [29], revealing the successful immobilization of Ab_2/SiO_2 on the foam through the sandwich immunoreaction. As expected, the 3d peak (368.1, 374.1 eV) of AgNPs [30] was only observed in curve iv since the AgNPs deposition was performed at the last step. Because the Ab_1, AFP and Ab_2/SiO_2, which applied in immobilization step (curve ii) and sandwich immunoreaction step (curve iii), were pre-dissolved in PBS, Na 1s (1,072 eV) and Na Auger (497 eV) peaks [31] were exhibited in curves ii and iii. These XPS results clearly show the occurrence of reactions outlined in Scheme 1.

The corresponding changes in surface morphologies of the immunosensor were monitored by SEM and shown in Fig. S2 (online). In addition, the interfacial electron-transfer resistance (R_{ct}) changes during the immunosensor fabrication and immunoassay process were also investigated by electrochemical impedance spectroscopy (EIS). As shown in Fig. 3a, both the bare foam (curve 1) and the Au-deposited foam (curve 2) exhibited very low R_{ct} because of their excellent conductivity. However, R_{ct} of the immunosensor (curve 3) increased due to the immobilization of the insulating Ab_1 and blocking BSA onto the 3D-G@Ni foam to hinder the electron-transfer. After immunoreaction with AFP (curve 4), R_{ct} increased obviously due to the bonding of a new insulating protein layer onto the 3D-G@Ni foam. Finally, when another new complex insulating SiO_2/Ab_2 layer was anchored on the 3D-G@Ni foam (curve 5), the R_{ct} further increased sharply.

The effects of different interfaces on the deposition of AgNPs were investigated by the LSV measurements. During the linear potential sweep, the deposited AgNPs showed a well-defined anodic stripping peak with a peak potential at about +0.10 V. Both the bare foam and Au-deposited foam can induce AgNPs deposition even without any reducing reagent, which can be seen from the Fig. 3b (curve 1, 2). However, the LSV curve of AgNPs formed at Au-deposited foam showed greater response than on bare foam, indicating AuNPs is an excellent inducer for the AgNPs deposition [19,28,32]. When Ab_1 and blocking BSA were combined to AuNPs to construct immunosensor (curve 3), the LSV curve response became lower than that of the Au-deposited foam (curve 2) because the free-active sites of AuNPs became less. After immunoreaction with AFP (curve 4), new insulating layer was formed on some area of the immunosensor, which would hinder the electron-transfer and the contact between Au-deposited foam and $AgNO_3$ for AgNPs to be deposited (Scheme 1). So, the LSV curve response showed further decrease after immunoreaction with AFP. For the same reason, when larger insulating complex, SiO_2/Ab_2 were anchored on the foam, the LSV curve response exhibited a further decrease (curve 5).

3.4. Optimization of detection conditions

The AgNPs deposition time is an important parameter affecting the analytical performance of immunoassay. At 5 min deposition, the LSV peak current of blank and AFP of 5.0 ng/mL solutions showed the highest difference (Fig. 4a), so 5 min was chosen as the optimal deposition time in immunoassay.

The incubation time for immunoreaction is another important parameter affecting the analytical performance of immunoassay. The time for AFP incubation was firstly optimized. The LSV peak current decreased with increasing AFP incubation time and trended to a constant value after an incubation time of 30 min (curve i, Fig. 4b). Longer time did not decrease the response, indicating 30 min was sufficient for saturated binding between AFP and Ab_1. However, for further saturated binding SiO_2/Ab_2 with analyte, 40 min was sufficient (curve ii, Fig. 4b). Because SiO_2/Ab_2 is bigger than AFP and needs longer time for binding reaction. Therefore, the optimal incubation time for AFP and SiO_2/Ab_2 were selected as 30 and 40 min, respectively.

The optimal concentration of Ab_1 on the interface of the immunosensor was also investigated. As shown in Fig. S3 (online), 10 μg/mL of the Ab_1 was chosen as the optimal concentration.

3.5. Analytical performance

Under optimum conditions, the LSV peak current of deposited AgNPs on the immunosensor decreased with increasing concentration of AFP in the incubation solution (Fig. 5a). The calibration plot showed a good linear relationship between the ratio of the analyte peak current to blank peak current (I/I_0) and the logarithm of AFP concentration (lgc) in the range from 5.0 pg/mL to 5.0 ng/mL. The linear regression equation was found to be $I/I_0 = 0.5095–0.1734$ lgc(ng/mL) with a correlation coefficient of 0.9980 (Fig. 5b). The limit detection was 2.3 pg/mL, which is much lower than many of electrochemical immunosensors with intricate signal amplifying strategy based on two-dimensional (2D) electrode [33–38].

Both the intra-assay and the inter-assay precisions of the immunosensor array were examined by parallel immunoassay for 5 times with AFP concentration of 0.5 ng/mL. The intra-assay relative standard deviation (RSD) was 4.83% and the inter-assay RSD was 6.78%. The results showed that the immunosensor had

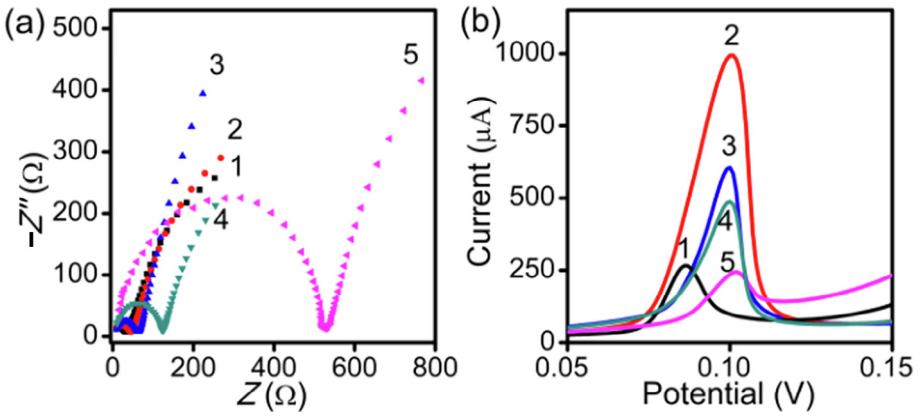

Fig. 3. (Color online) (a) EIS and (b) LSV curves of AgNPs of different interfaces: (1) foam, (2) Au-deposited foam, (3) after the Ab_1 immobilization, (4) after immunoreaction with 5.0 ng/mL AFP, (5) further immunoreaction with SiO_2/Ab_2.

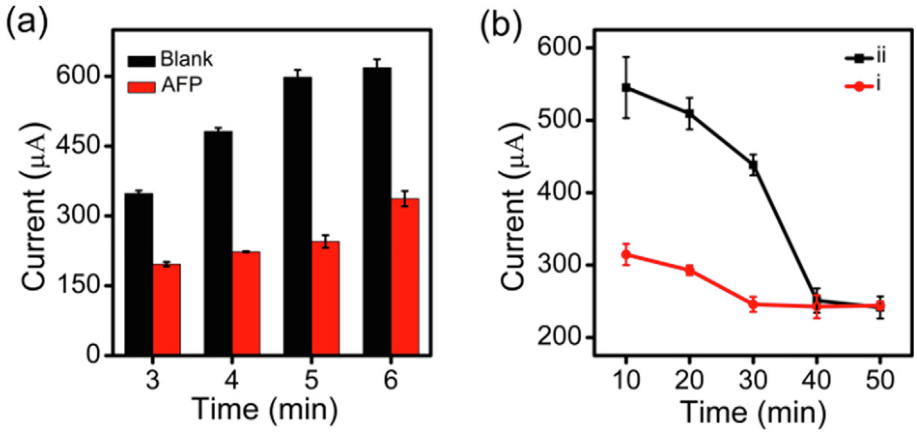

Fig. 4. (Color online) The optimal conditions for immunoassay (a) Ag deposition time, (b) sandwich immunoreaction time for AFP (i) and Ab_2/SiO_2 (ii). The concentrations of Ab_1, AFP, SiO_2/Ab_2 were 10 μg/mL, 5 ng/mL and 10 μg/mL (according to the Ab_2 amount used for preparing nanotag), respectively.

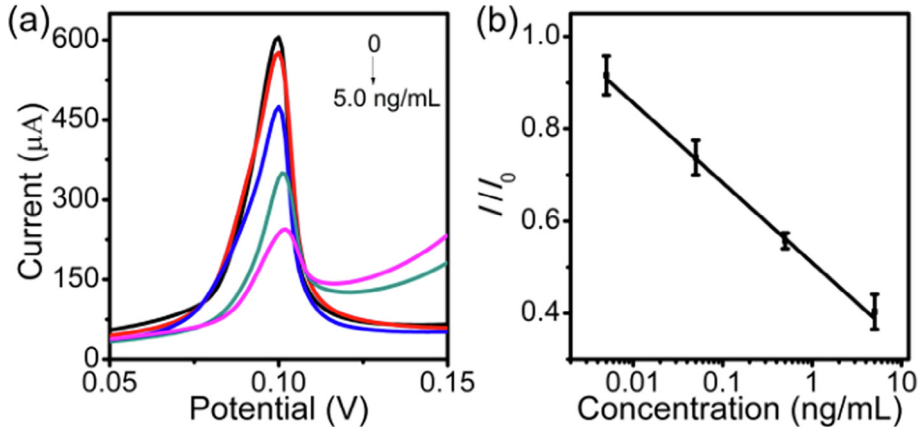

Fig. 5. (Color online) (a) LSV responses of the immunosensor toward AFP at different concentrations and (b) the calibration curve of the immunoassay method.

good precision and acceptable fabrication reproducibility. In addition, 91.03% of the initial response was remained after the immunosensor was stored dry at 4 °C for 1 week, indicating an acceptable stability.

The selectivity of the immunosensor was also investigated using P53, MIgG and GO_x as analytes. As shown in Fig. S4 (online), no obvious current decrease over the blank control was observed when these noncognate proteins were used for the sandwich immunoassay in the immunosensor. However, the target protein of AFP showed an obvious current decrease. These results indicated that the immunosensor had a good selectivity.

3.6. Application in analysis of serum samples

To evaluate the reliability and application potential of the newly-developed immunosensor, we used the present immunosensor to determine AFP in clinical human serum samples in comparison with the reference values supplied by the Second Affiliated Hospital of Wenzhou Medical University. The samples were diluted by 10 times with 0.01 mol/L pH 7.4 PBS prior to assay and then determined according to the immunoassay procedure (Section 2.6). The final calculation results were shown in Table 1. Comparing with the results supplied by the hospital, the present immunosensor exhibited an acceptable agreement with relative errors less than 8.68%, indicating a suitable reliability for the clinical testing.

Table 1
Comparison of the AFP measurements in clinical serum samples using the newly-developed and reference methods (ng/mL).

Sample no.	1	2	3
Newly-developed method	2.21 ± 0.17	1.84 ± 0.12	4.19 ± 0.05
Reference method[a]	2.42	1.79	4.04
Relative error (%)	−8.68%	2.79%	3.71%

[a] The reference values were obtained from electrochemiluminescent tests on commercial automation electrochemiluminescent analyzer (Elecsys 2010, Roche) and supplied by the Second Affiliated Hospital of Wenzhou Medical University.

4. Conclusions

Using monolithic 3D-G@Ni foam as a free-standing electrode, we have developed a simple disposable 3D-immunosensor by sequentially SEED-depositing gold nanoparticles (AuNPs) for immobilization of antibody (Ab_1) and silver nanoparticles (AgNPs) for electrochemical stripping detection. Without involving any reducing reagent, this reported methodology is cost/energy effective, rapid and eco-friendly. Unlike other sensors with a 3D-graphene foam electrode, we kept the Ni substrate because Ni was found to show no electrochemical signal at 0.10 V, which is the stripping peak potential for the deposited AgNPs in 1.0 mol/L KCl solution. As such, the Ni-foam-templated electrode can keep excellent mechanical properties attractive for the fabrication of disposable immunosensors. Furthermore, the Ni foam template

can support the electroless deposition of AuNPs and AgNPs on the electrode. The AuNPs deposited on the 3D-G@Ni foam could be used as a linker for immobilization biomolecular on the 3D foam, which overcame the difficulty for biofunctionalization of 3D-graphene. The newly-developed sensor showed a wide linear response to a module analyte of α-fetoprotein antigen (AFP), ranging from 5.0 pg/mL to 5.0 ng/mL and a low detection limit down to 2.3 pg/mL. This 3D-immunosensor is sensitive, reliable, and easy to make, showing great potential for clinic applications.

Conflict of interest

The authors declare that they have no conflict of interest.

Acknowledgments

This work was financially supported by the Natural Science Foundation of Zhejiang Province (LY18H200008), Wenzhou Science and Technology Bureau Project (Y20170203), and National Natural Science Foundation of China (51433005).

Author contributions

C.Z. designed the experimental scheme and performed the determination of AFP. X.L. and S.A. fabricated the electrodes. D.Z., S.P. and X.Z. carried out the SEM, Raman and FTIR characterization, respectively. Y.L. and Q.Y. synthesized the graphene@Ni foam. M.Y. prepared the SiO_2 nanospheres. L.D. contributed the idea, supervised the study, and wrote up the manuscript together with C.Z.

Appendix A. Supplementary data

Supplementary data to this article can be found online at https://doi.org/10.1016/j.scib.2019.07.015.

References

[1] Tang Z, Ma Z. Multiple functional strategies for amplifying sensitivity of amperometric immunoassay for tumor markers: a review. Biosens Bioelectron 2017;98:100–12.
[2] Zhao C, Wu J, Ju H, et al. Multiplexed electrochemical immunoassay using streptavidin/nanogold/carbon nanohorn as a signal tag to induce silver deposition. Anal Chim Acta 2014;847:37–43.
[3] Verma S, Singh A, Shukla A, et al. Anti-IL8/AuNPs-rGO/ITO as an immunosensing platform for noninvasive electrochemical detection of oral cancer. ACS Appl Mater Interfaces 2017;9:27462–74.
[4] Zhang Q, Li L, Qiao Z, et al. Electrochemical conversion of Fe_3O_4 magnetic nanoparticles to electroactive prussian blue analogues for self-sacrificial label biosensing of avian influenza virus H5N1. Anal Chem 2017;89:12145–51.
[5] Habtamu HB, Sentic M, Silvestrini M, et al. A sensitive electrochemiluminescence immunosensor for celiac disease diagnosis based on nanoelectrode ensembles. Anal Chem 2015;87:12080–7.
[6] Li B, Liu J, Zhou H. Amplified fluorescence detection of serum prostate specific antigen based on metal-dependent DNAzyme assistant nanomachine. Anal Chim Acta 2018;1008:96–102.
[7] Virzonis D, Vanagas G, Ramanaviciene A, et al. Resonant gravimetric immunosensing based on capacitive micromachined ultrasound transducers. Microchim Acta 2014;181:1749–57.
[8] Patrie SM, Mrksich M. Self-assembled monolayers for MALDI-TOF mass spectrometry for immunoassays of human protein antigens. Anal Chem 2007;79:5878–87.
[9] Wen W, Yan X, Zhu C, et al. Recent advances in electrochemical immunosensors. Anal Chem 2017;89:138–56.
[10] Ricci F, Adornetto G, Palleschi G. A review of experimental aspects of electrochemical immunosensors. Electrochim Acta 2012;84:74–83.
[11] Wang B, Akiba U, Anzai JI. Recent progress in nanomaterial-based electrochemical biosensors for cancer biomarkers: a review. Molecules 2017;22:1048.
[12] Felix FS, Angnes L. Electrochemical immunosensors - a powerful tool for analytical applications. Biosens Bioelectron 2018;102:470–8.
[13] Dong X, Wang X, Wang L, et al. 3D graphene foam as a monolithic and macroporous carbon electrode for electrochemical sensing. ACS Appl Mater Interfaces 2012;4:3129–33.
[14] Guo J, Zhang T, Hu C, et al. A three-dimensional nitrogen-doped graphene structure: a highly efficient carrier of enzymes for biosensors. Nanoscale 2015;7:1290–5.
[15] Liu J, Wang X, Wang T, et al. Functionalization of monolithic and porous three-dimensional graphene by one-step chitosan electrodeposition for enzymatic biosensor. ACS Appl Mater Interfaces 2014;6:19997–20002.
[16] Yao Q, Jing J, Zeng Q, et al. Bilayered BMP2 eluting coatings on graphene foam by electrophoretic deposition: electroresponsive BMP2 release and enhancement of osteogenic differentiation. ACS Appl Mater Interfaces 2017;9:39962–70.
[17] Liu J, Wang J, Wang T, et al. Three-dimensional electrochemical immunosensor for sensitive detection of carcinoembryonic antigen based on monolithic and macroporous graphene foam. Biosens Bioelectron 2015;65:281–6.
[18] Qu L, Dai L. Substrate-enhanced electroless deposition of metal nanoparticles on carbon nanotubes. J Am Chem Soc 2005;127:10806–7.
[19] Park SJ, Taton TA, Mirkin CA. Array-based electrical detection of DNA with nanoparticle probes. Science 2002;295:1503–6.
[20] Wu Y, Chen C, Liu S. Enzyme-functionalized silica nanoparticles as sensitive labels in biosensing. Anal Chem 2009;81:1600–7.
[21] Lai G, Wu J, Leng C, et al. Disposable immunosensor array for ultrasensitive detection of tumor markers using glucose oxidase-functionalized silica nanosphere tags. Biosens Bioelectron 2011;26:3782–7.
[22] Feng X, Zhang Y, Zhou J, et al. Three-dimensional nitrogen-doped graphene as an ultrasensitive electrochemical sensor for the detection of dopamine. Nanoscale 2015;7:2427–32.
[23] Ronkainen NJ, Halsall HB, Heineman WR. Raman spectrum of graphene and graphene layers. Chem Soc Rev 2010;39:1747–63.
[24] Chen Z, Ren W, Gao L, et al. Three-dimensional flexible and conductive interconnected graphene networks grown by chemical vapour deposition. Nat Mater 2011;10:424–8.
[25] Ferrari AC, Basko DM. Raman spectroscopy as a versatile tool for studying the properties of graphene. Nat Nanotechnol 2013;8:235–46.
[26] Tang Z, Wang L, Ma Z. Triple sensitivity amplification for ultrasensitive electrochemical detection of prostate specific antigen. Biosens Bioelectron 2017;92:577–82.
[27] Zhang X, Shi H, Xu B. Catalysis by gold: isolated surface Au^{3+} ions are active sites for selective hydrogenation of 1,3-butadiene over Au/ZrO_2 catalysts. Angew Chem Int Ed 2005;44:7132–5.
[28] Lin D, Wu J, Wang M, et al. Triple signal amplification of graphene film, polybead carried gold nanoparticles as tracing tag and silver deposition for ultrasensitive electrochemical immuno-sensing. Anal Chem 2012;84:3662–8.
[29] Zhong B, Song L, Huang X, et al. Novel coaxial SiC–SiO_2–BN nanocable: large-scale synthesis, formation mechanism and photoluminescence property. J Mater Chem 2011;21:14432–40.
[30] Prieto P, Nistor V, Nouneh K, et al. XPS study of silver, nickel and bimetallic silver–nickel nanoparticles prepared by seed-mediated growth. Appl Surf Sci 2012;258:8807–13.
[31] Moreira GF, Peçanha ER, Monte MBM, et al. XPS study on the mechanism of starch-hematite surface chemical complexation. Miner Eng 2017;110:96–103.
[32] Lin D, Mei C, Liu A, et al. Cascade signal amplification for electrochemical immunosensing by integrating biobarcode probes, surface-initiated enzymatic polymerization and silver nanoparticle deposition. Biosens Bioelectron 2015;66:177–83.
[33] Zhao Y, Zheng Y, Kong R, et al. Ultrasensitive electrochemical immunosensor based on horseradish peroxidase (HRP)-loaded silica-poly(acrylic acid) brushes for protein biomarker detection. Biosens Bioelectron 2016;75:383–8.
[34] Liu J, Lin G, Xiao C, et al. Sensitive electrochemical immunosensor for α-fetoprotein based on graphene/SnO_2/Au nanocomposite. Biosens Bioelectron 2015;71:82–7.
[35] Yuan Y, Li S, Xue Y, et al. A Fe_3O_4@Au-basedpseudo-homogeneous electrochemical immunosensor for AFP measurement using AFP antibody-GNPs-HRP as detection probe. Anal Biochem 2017;534:56–63.
[36] Wang Z, Liu N, Feng F, et al. Synthesis of cadmium, lead and copper alginate nanobeads as immunosensing probes for the detection of AFP, CEA and PSA. Biosens Bioelectron 2015;70:98–105.
[37] Alizadeh N, Salimi A, Hallaj R. Magnetoimmunosensor for simultaneous electrochemical detection of carcinoembryonic antigen and α-fetoprotein using multifunctionalized Au nanotags. J Electroanal Chem 2018;811:8–15.
[38] Tu M, Chen H, Wang Y, et al. Immunosensor based on carbon nanotube/manganese dioxide electrochemical tags. Anal Chim Acta 2015;853:228–33.

Changrong Zhao received her B.S. degree from Hebei University in 2004. From 2004 to 2015, she worked in Wenzhou Medical University as a teacher. In 2015, she became a Ph.D. student at Institute of Advanced Materials for Nano-Bio Applications, Wenzhou Medical University. Her research interests mainly focus on the biosensors based on nanomaterials and nanoengineering.

Liming Dai joined Case Western Reserve University in 2009 as the Kent Hale Smith Professor in the Department of Macromolecular Science and Engineering. He is also director of the Center of Advanced Science and Engineering for Carbon (CASE4Carbon) and honorary director of the Institute of Advanced Materials for Nano-Bio Applications. His expertise covers the synthesis, functionalization, and device fabrication of polymers and carbon nanomaterials for energy and bio-related applications.